 doi:10.20944/preprints202002.0057.v1

Communication

Hierarchically Porous Silk/Activated-Carbon Composite Fibers for Adsorption and Repellence of Volatile Organic Compounds

Aled D. Roberts[1,2], Jet-Sing M. Lee[3], Adrián Magaz[1], Martin W. Smith[4], Michael Dennis[4], Nigel S. Scrutton[2] and Jonny J. Blaker[1,2]*

[1] Bio-Active Materials Group, Department of Materials & Henry Royce Institute, The University of Manchester, Manchester, M13 9PL, UK; jonny.blaker@manchester.ac.uk
[2] Future Biomanufacturing Research Hub (FBRH), Manchester Institute of Biotechnology, The University of Manchester, Manchester, M1 7DN, UK; nigel.scrutton@manchester.ac.uk
[3] Institute for Integrated Cell-Material Sciences, Institute for Advanced Study, Kyoto University, Yoshida, Sakyo-ku, Kyoto, 606-8501, Japan
[4] Defence Science and Technology Laboratory (Dstl), Porton Down, Salisbury, SP4 0JQ, UK
* Correspondence: jonny.blaker@manchester.ac.uk; Tel.: +44-0161-306-3587

Abstract: Fabrics comprised of porous fibers could provide effective passive protection against chemical and biological (CB) threats whilst maintaining high air permeability (breathability). Here, we fabricate hierarchically porous fibers consisting of regenerated silk fibroin (RSF) and activated-carbon (AC) prepared through two fiber spinning techniques in combination with ice-templating – namely cryogenic solution blow spinning (Cryo-SBS) and cryogenic wet-spinning (Cryo-WS). The Cryo-WS RSF fibers had exceptionally small macropores (as low as 0.1 μm) and high specific surface areas (SSAs) of up to 79 $m^2 g^{-1}$. The incorporation of AC could further increase the SSA to 210 $m^2 g^{-1}$ (25 wt. % loading) whilst also increasing adsorption capacity for volatile organic compounds (VOCs).

Keywords: porous fibers, activated carbon, ice-templating, ice segregation induced self-assembly, silk fibroin, wet spinning, solution blow spinning

1. Introduction

The current generation of air-permeable chemical and biological (CB) resistant clothing, such as Joint Service Lightweight Integrated Suit Technology (JSLIST), consists of a particulate activated carbon (AC) adsorbent layer laminated between multiple layers of fabric – including a hydrophobic outer layer and soft inner layer.[1,2] Combining the properties of these layers into a single material could reduce the physiological burden on the user through mass reduction and enhanced diffusive and evaporative heat transport. Fabrics comprised of porous fibers with a significant capacity to adsorb and repel volatile organic compounds (VOCs) could help achieve this goal. In particular, a hierarchical structure of pores – where networks of larger macropores (>50 nm) provide effective diffusion and access to smaller meso- (2 – 50 nm) and micropores (<2 nm) – could provide effective rapid adsorption activity whilst maintaining high permeability and relatively low mass.[3] Furthermore, fibers with micron-scale surface features could also enhance liquid repellence through a 'lotus-leaf' type effect – repelling liquid VOC droplets as well as dirt, dust and mud.[4]

Although other highly porous materials such as metal organic frameworks (MOFs) and silicates have demonstrated exceptional adsorption and degradation activity against various chemical warfare agents (CWAs),[1,5–7] their relatively poor chemical and physical stability and high cost of manufacture mean they are unlikely to replace low-cost ACs (which can also effectively catalyze the degradation of CWAs[8]) for general applications. The brittle nature and poor mechanical properties of microporous materials such as ACs, MOFs and silicates make them unsuitable for use as stand-

Preprints (www.preprints.org) | NOT PEER-REVIEWED | Posted: 5 February 2020 doi:10.20944/preprints202002.0057.v1

alone materials in fabrics; instead, they need to be combined with another material with suitable physical properties in order to be incorporated into a garment. This can be achieved by decorating the surface of fibers with a porous material,[1,5,6] but loss of physical attachment means durability can be a significant issue.

In this work, we reprocess silkworm silk into aqueous regenerated silk fibroin (RSF) solutions before spinning into porous fibers *via* two cryogenic spinning techniques, namely Cryogenic Solution Blow Spinning (Cryo-SBS) and Cryogenic Wet Spinning (Cryo-WS). Cryogenically freezing hydrated fibers results in ice-segregation-induced self-assembly (ISISA) which, after freeze-drying, produces a macroporous ice-templated structure (Figure 1).[9–18] By spinning colloidal suspensions of AC in RSF, macroporous fibers loaded with AC can be obtained – increasing the specific surface area (SSA), hydrophobicity and adsorption capacity for VOCs. A summary of the conditions employed to prepare samples, along with the most relevant physical properties, is given in Table 1.

Table 1. Summary of the physical properties of the porous RSF and RSF/AC fibers produced. Approximate fiber and macropore diameters (Ø) determined through analysis of SEM images.

Method	AC loading [wt. %]	Approx. fiber Ø [μm]	Approx. macropore Ø [μm]	N_2 BET SSA [m^2 g^{-1}]	Accessible SSA [%]	Micropore vol. [cm^3 g^{-1}]	Max. cyclohexane uptake [w/w %]
(AC only)	100	n/a	n/a	697	100	0.358	22.8
Cryo-SBS	0	70	0.9 – 5	34	100	0.038	n/a
Cryo-SBS	4	26	0.9 – 4.4	17	28	0.015	n/a
Cryo-SBS	10	100	10 – 15	44	44	0.051	n/a
Cryo-WS	0	160	0.2 – 2	79	100	0.032	12.9
Cryo-WS	10	180	0.05 – 5	121	86	0.035	26.6
Cryo-WS	15	100	0.1 – 5	134	79	0.018	27.0
Cryo-WS	20	150	0.1 – 10	143	71	0.047	25.5
Cryo-WS	25	200	0.2 - 1	210	90	0.156	22.4

2. Results

RSF spinning dopes were prepared following a previously published protocol detailed in the SI.[11,19] Porous RSF fibers were prepared *via* Cryo-SBS (Figure 1a) following a protocol previously developed within our group,[10,11,20] however the Cryo-WS method (Figure 1b) has, to the authors' knowledge, not been reported previously. For the Cryo-SBS method, RSF and colloidal RSF-AC mixtures were spun directly into a liquid nitrogen (LN_2) bath, collected and freeze dried (Figure 1a). This rapid freezing induces the formation of macropores *via* ISISA.[9–14] The obtained fibers were approximately 0.2 – 1 cm in length and 25 – 100 μm in diameter, and darkened uniformly with increasing AC content (Figure 1c). Their relatively short length meant they would unsuitable for processing into a woven fabric, but could potentially be employed as a non-woven material (*i.e.*, a felt). Scanning electron microscopy (SEM) imaging revealed macropores ranging from 1 – 15 μm in diameter (Figure 1c), which are fairly small for a freeze-casting method – which typically produces pores in the range of 5 – 50 μm.[21,22] The relatively small pores are likely due to rapid freezing from the high surface area-to-volume ratio of the fibers and high temperature differential between the fibers and LN_2, since pore size from freeze-casting methods are inversely proportional to the velocity of ice crystal growth.[22] It can also be seen from the SEM images that the fibers have a seemingly non-porous outer sheath. This likely arises from evaporation-induced phase separation at the surface of the fiber as it travels through the air gap between the nozzle and the cryogenic bath; a phenomenon

Preprints (www.preprints.org) | NOT PEER-REVIEWED | Posted: 5 February 2020 doi:10.20944/preprints202002.0057.v1

also observed for some dry-jet wet spun fibers.[23] For the Cryo-WS method, RSF and colloidal RSF-AC mixtures were wet-spun into an ethanol coagulation bath akin to previous literature reports for wet-spun RSF fibres (Figure 1b).[24–28] The wet fibers were then subjected to solvent exchange in deionised (DI) water, before being rapidly frozen by submersion in LN_2 followed by freeze-drying. The dry fibers were continuous in length and had a diameter of 100 – 300 µm (Figure 1d); smaller diameter fibers could feasibly be produced by employing a smaller diameter extrusion nozzle or by employing post-spin drawing. The fibers were fairly flexible to handle and also darkened with increasing AC content. The fibers had macropores ranging from 0.1 – 10 µm, which – to the author's knowledge – are the smallest reported for an ice-templating based method (where water is the solvent). This is likely due to the rapid freezing resulting in relatively small ice crystals and hence small pores after freeze-dying.[22] Xia and co-workers produced porous fibres with similarly small (~0.1 µm) macropores *via* a cryogenic electrospinning technique (employing organic solvents rather than water), suggesting a similar underlying pore formation mechanism.[13]

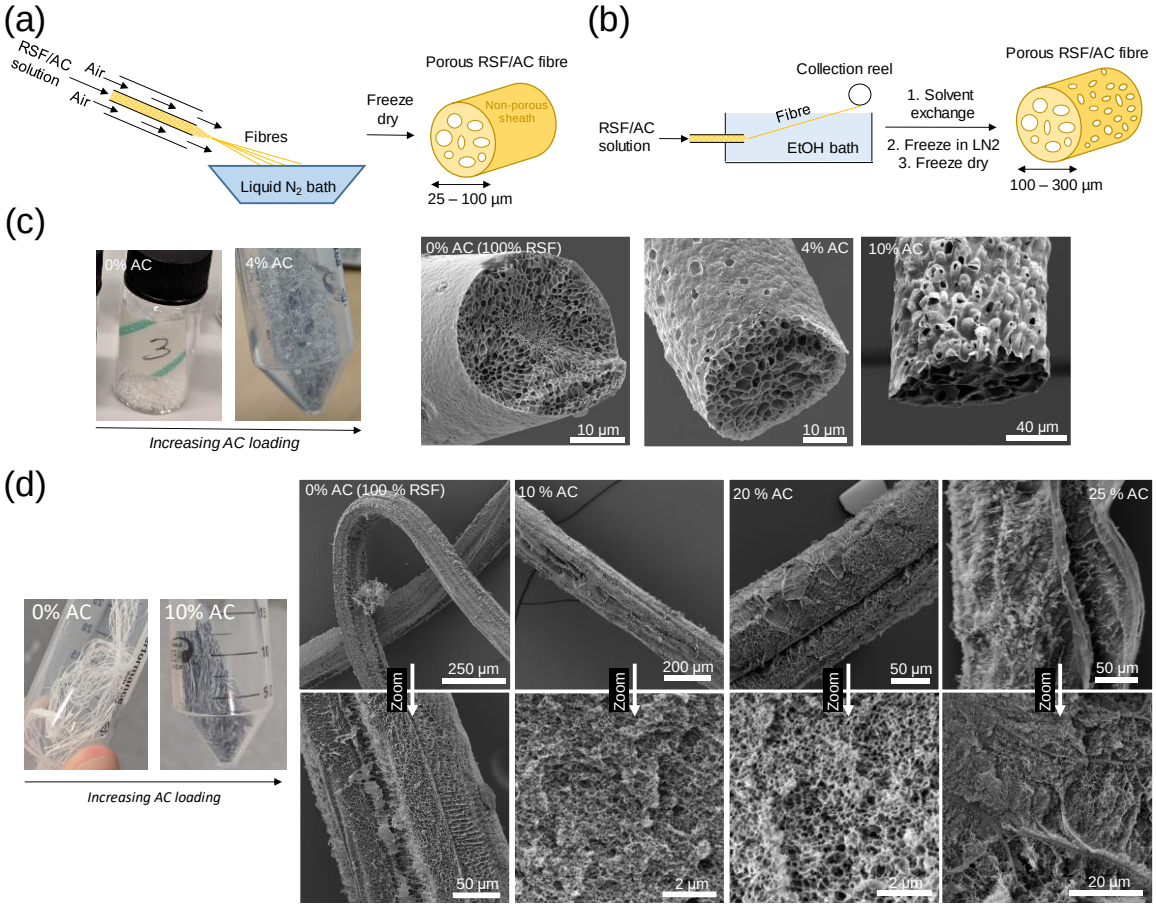

Figure 1. Schematic representation of (**a**) the Cryo-SBS and (**b**) the Cryo-WS fiber spinning rigs. (**c**) Visible light and SEM images of RSF fibers produced by Cryo-SBS with increasing AC loading (left to right, 0, 4 and 10 wt. %). (**d**) Visible light and SEM images of RSF fibers produced by Cryo-WS with increasing AC loading (left to right, 0, 10, 20 and 25 wt. %)

The SSA and micropore volume of the fibers were determined through N_2 gas sorption and Brunauer-Emmett-Teller (BET) analysis (Figure 2 and Table 1). The surface area of the Cryo-SBS fibers with 0% AC was 34 $m^2 g^{-1}$, which is fairly high for ISISA-derived pores which typically have SSAs less than 15 $m^2 g^{-1}$.[21,22] This relatively high surface area is likely a result of the relatively small macropores as observed by SEM. A 4% AC loading saw a decrease in SSA to 17 $m^2 g^{-1}$, only 28% of the theoretical SSA considering the masses of the silk (at 34 $m^2 g^{-1}$) and AC (at 697 $m^2 g^{-1}$) individually, suggesting that most pores were inaccessible. A 10% AC loading yielded an SSA of 44 $m^2 g^{-1}$, which was 44% of the theoretical SSA (100 $m^2 g^{-1}$). This relatively poor performance could be attributed to the outer non-porous sheath restricting gaseous diffusion to the AC, or rapid freezing resulting in smothering of

Preprints (www.preprints.org) | NOT PEER-REVIEWED | Posted: 5 February 2020 doi:10.20944/preprints202002.0057.v1

the AC particles within the RSF polymer. Analysis of the isotherms revealed an increase in micropore volume from 0.038 to 0.05 $cm^3\ g^{-1}$ with a 10% AC loading, suggesting the increase in SSA was largely from the microporous AC. The Cryo-WS fibers with 0% AC had a significantly higher SSA at 79 $m^2\ g^{-1}$ which – to the best of our knowledge – is the highest reported SSA for an ice-templated polymeric material. Incorporation of AC gradually increased the SSA to a maximum value of 210 $m^2\ g^{-1}$ with a 25% AC loading – corresponding to an accessible surface area of 90% (Figure 2c). Use of ACs with higher SSAs (the employed AC had a SSA of 697 $m^2\ g^{-1}$, but some ACs can exceed 4000 $m^2\ g^{-1}$)[29] or other highly microporous materials such as MOFs would likely result in fibers with significantly higher SSAs.

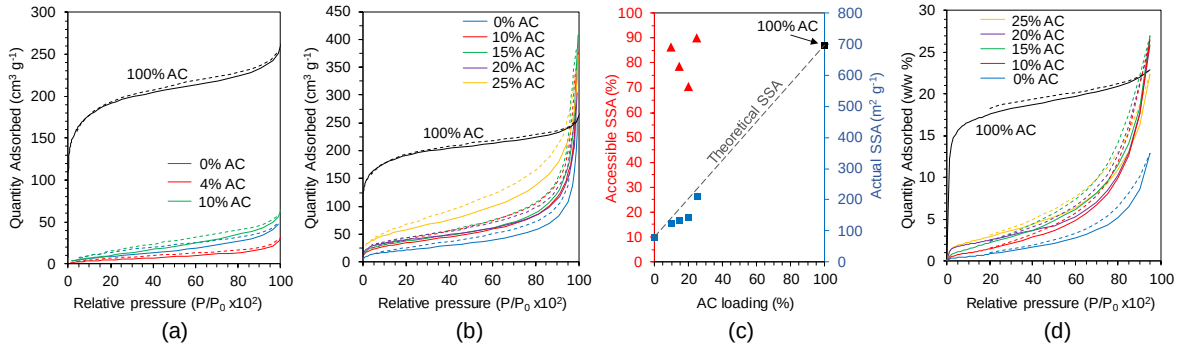

Figure 2. N_2 gas sorption isotherms for porous RSF fibers produced by (a) Cryo-SBS with 0, 4 and 10 wt. % AC loading and (**b**) Cryo-WS with 0, 10, 15, 20 and 25 wt. % AC loading. Dashed lines indicate desorption, 100% AC included for comparison. (**c**) Relationship between AC loading and both % accessible SSA and actual SSA for RSF fibers produced by Cryo-WS. (**d**) Cyclohexane adsorption isotherms for RSF fibers produced through Cryo-WS with 0 – 25 wt. % AC loading. 100% AC included for comparison.

The efficacy of the fibers for adsorption of VOCs was assessed through Dynamic Vapour Sorption (DVS); here, cyclohexane was employed as a representative VOC for proof of principle. Porous fibers produced *via* Cryo-WS displayed significant adsorption capacity for VOCs (Table 1, Figure 2d.), with the majority of adsorption occurring at relatively high partial pressures – suggesting macropores from ISISA were largely contributing to adsorption rather than micropores from the AC. This was corroborated by the fact that an increase in AC loading from 10% to 25% had little effect on cyclohexane adsorption, although 0% AC loading had a smaller adsorption capacity. No significant cyclohexane adsorption could be detected for the Cryo-SBS fibers however, possibly due their lower SSAs or the presence of the non-porous sheath outer restricting diffusion to the porous core.

The mechanical properties for the fibers were investigated through uniaxial tensile testing (Figure S1), however the highly porous nature of the fibers meant the true cross-sectional surface area of the fibers (needed to convert force to stress) could not be accurately determined, and therefore calculation of the tensile strength was not possible. Contact angle measurements on RSF fiber mats produced by Cryo-SBS with 0% and 4% AC loading revealed increased hydrophobicity with an increasing AC content (Figure S2.). This is likely due to relatively hydrophobic AC on the surface of the fibers reducing their wettability, but may also be a result of enhanced surface roughness causing a "lotus-leaf" type repellence effect (Figure S2c.) – a more in depth study is needed to confirm this possibility however. Contact angle data could not be obtained for Cryo-WS fibers since their relatively bulky nature meant adequately uniform mats could not be produced. Visible light and cross-polarised microscopy was also performed on the fibers to visualise the distribution of AC; a technique which was recently employed to visualise the distribution of graphene within hollow aramid fibers (Figure S3.).[30] This revealed a fairly uniform distribution of AC within the fibers (*i.e.* no significant agglomeration observed).

The composition and microstructure of the dry fibers was analysed through wide angle X-ray diffraction (WAXD) and Fourier-transform infrared spectroscopy (FTIR). Natural silk has a

 doi:10.20944/preprints202002.0057.v1

polycrystalline structure arising from ordered β-sheet domains, which has also been observed in some RSF-derived materials.[24–26] The obtained WAXD patterns were, however, indistinguishable from a background measurement, suggesting low crystallinity within these porous fibers (Figure S4). The high void volume in the porous fibers could also account for the low WAXD signal strength. FTIR was employed to probe the protein secondary structure of the RSF fibers through analysis of the amide I region of the spectrum (1600 – 1700 cm^{-1}), allowing determination of the relative percentage of secondary structural features (*i.e.* random coils, α-helixes, β-sheets and β-turns). This revealed a high content of amorphous features relative to crystalline β-sheets, in concordance with the WAXD data. Post-treatment of the RSF fibers with ethanol, which has been shown to induce β-sheet formation,[11] was also performed – resulting in a significant increase (approx. 1.7 fold) in β-sheet features for the porous RSF fibers from both fiber spinning techniques. Post-treatment with ethanol could therefore be exploited to moderate the mechanical properties of the fibres, since a higher β-sheet content typically results in stronger, stiffer fibers.[31]

3. Conclusions

In this work, hierarchically porous RSF fibers loaded with AC were produced through two cryogenic fiber spinning techniques – namely Cryo-SBS and a novel Cryo-WS method. Both of these techniques produced fibers with significantly different properties; notably Cryo-SBS fibers had a porous core and non-porous outer sheath which likely restricted gaseous diffusion, compromising accessible SSA and hence VOC adsorption capacity, these fibre were also discontinuous in length. Cryo-WS fibers, on the other hand, were continuous in length and porous throughout, with exceptionally small macropores for an ice-templating method (*c.a.* 0.1 μm) with significant VOC adsorption capacity. Further refinement of the spinning techniques may produce mesoporous (0.05 μm) fibers with further improved VOC adsorption, and the use of ultra-high surface area ACs or other microporous materials may also offer improvements. With further development, fibers such as these could be incorporated into woven or non-woven materials where their hierarchically porous structure in tandem with high VOC adsorption capacity could provide passive protection against CWAs or other airborne toxins. Porous RSF fibres such as these could have applications in a range of fields, particularly tissue regeneration and controlled drug delivery.[32–35] Finally, the use of genetically engineered silks such as recombinant spider silk could tune the mechanical and textural properties of the silk, or introduce chemical functionality such as additional lysine groups ($-NH_2$) to neutralise toxic VOCs or other substances.[36]

Supplementary Materials: The following are available online at www.mdpi.com/xxx/s1, Materials and methods, Figure S1, Figure S2, Figure S3, Figure S4, Figure S5, Video S1 and Video S2.

Author Contributions: Conceptualization, A. D. R. and J. J. B.; methodology, A. D. R.; characterization and analysis, A. D. R., J-S. M. L, A. M., M. W. S.; writing (original draft preparation), A. D. R.; reviewing and editing, all authors; supervision and project administration, J. J. B, M. D., N. S. S. All authors have read and agreed to the published version of the manuscript.

Funding: This work was funded by DSTL project no. CDE100640 and DSTLX1000101893, with support from the EPSRC/BBSRC Future Biomanufacturing Research Hub (EP/S01778X/1). We also acknowledge the SYNBIOCHEM center (grant No. BB/M017702/1) and Henry Royce Institute for Advanced Materials (EP/R00661X/1, EP/S019367/1, EP/P025021/1 and EP/P025498/1) for support and equipment use.

Acknowledgments: We kindly acknowledge Mr. Stuart Morse for assistance with mechanical testing and The University of Manchester X-Ray Diffraction Laboratory (Department of Materials) for assistance with WAXD.

Conflicts of Interest: The authors declare no conflict of interest.

 doi:10.20944/preprints202002.0057.v1

References

1. Johnson, B.J.; Melde, B.J.; Moore, M.H.; Taft, J.R. Deposition of porous sorbents on fabric supports. *J. Vis. Exp.* **2018**, 57331.
2. Levine, L.; Johnson, R.F.; Teal Jr, W.B.; Cadarette, B.S.; Merullo, D.J. Joint Service Lightweight Integrated Suit Technology Program: Heat Strain Evaluation in an Environmental Chamber and in the Field [Technical Report] 1998, 1–112.
3. Roberts, A.D.; Li, X.; Zhang, H. Porous carbon spheres and monoliths: morphology control, pore size tuning and their applications as Li-ion battery anode materials. *Chem. Soc. Rev.* **2014**, *43*, 4341–4356.
4. Ensikat, H.J.; Ditsche-Kuru, P.; Neinhuis, C.; Barthlott, W. Superhydrophobicity in perfection: the outstanding properties of the lotus leaf. *Beilstein J. Nanotechnol.* **2011**, *2*, 152–161.
5. López-Maya, E.; Montoro, C.; Rodríguez-Albelo, L.M.; Aznar Cervantes, S.D.; Lozano-Pérez, A.A.; Cenís, J.L.; Barea, E.; Navarro, J.A.R. Textile/Metal–Organic-Framework Composites as Self-Detoxifying Filters for Chemical-Warfare Agents. *Angew. Chemie Int. Ed.* **2015**, *54*, 6790–6794.
6. Zhao, J.; Losego, M.D.; Lemaire, P.C.; Williams, P.S.; Gong, B.; Atanasov, S.E.; Blevins, T.M.; Oldham, C.J.; Walls, H.J.; Shepherd, S.D.; et al. Highly Adsorptive, MOF-Functionalized Nonwoven Fiber Mats for Hazardous Gas Capture Enabled by Atomic Layer Deposition. *Adv. Mater. Interfaces* **2014**, *1*, 1400040.
7. Liu, Y.; Howarth, A.J.; Vermeulen, N.A.; Moon, S.-Y.; Hupp, J.T.; Farha, O.K. Catalytic degradation of chemical warfare agents and their simulants by metal-organic frameworks. *Coord. Chem. Rev.* **2017**, *346*, 101–111.
8. Columbus, I.; Waysbort, D.; Shmueli, L.; Nir, I.; Kaplan, D. Decomposition of Adsorbed VX on Activated Carbons Studied by 31P MAS NMR. *Environ. Sci. Technol.* **2006**, *40*, 3952–3958.
9. Gutiérrez, M.C.; Ferrer, M.L.; del Monte, F. Ice-Templated Materials: Sophisticated Structures Exhibiting Enhanced Functionalities Obtained after Unidirectional Freezing and Ice-Segregation-Induced Self-Assembly. *Chem. Mater.* **2008**, *20*, 634–648.
10. Medeiros, E.L.G.; Braz, A.L.; Porto, I.J.; Menner, A.; Bismarck, A.; Boccaccini, A.R.; Lepry, W.C.; Nazhat, S.N.; Medeiros, E.S.; Blaker, J.J. Porous Bioactive Nanofibers via Cryogenic Solution Blow Spinning and Their Formation into 3D Macroporous Scaffolds. *ACS Biomater. Sci. Eng.* **2016**, *2*, 1442–1449.
11. Magaz, A.; Roberts, A.D.; Faraji, S.; Nascimento, T.R.L.; Medeiros, E.S.; Zhang, W.; Greenhalgh, R.D.; Mautner, A.; Li, X.; Blaker, J.J. Porous, Aligned, and Biomimetic Fibers of Regenerated Silk Fibroin Produced by Solution Blow Spinning. *Biomacromolecules* **2018**, *19*, 4542–4553.
12. Scotti, K.L.; Dunand, D.C. Freeze casting – A review of processing, microstructure and properties via the open data repository, FreezeCasting.net. *Prog. Mater. Sci.* **2018**, *94*, 243–305.
13. McCann, J.T.; Marquez, M.; Xia, Y. Highly Porous Fibers by Electrospinning into a Cryogenic Liquid. *J. Am. Chem. Soc.* **2006**, *128*, 1436–1437.
14. Zhang, H.; Hussain, I.; Brust, M.; Butler, M.F.; Rannard, S.P.; Cooper, A.I. Aligned two-and three-dimensional structures by directional freezing of polymers and nanoparticles. *Nat. Mater.* **2005**, *4*, 787.
15. Deville, S. Ice-templating, freeze casting: Beyond materials processing. *J. Mater. Res.* **2013**, *28*, 2202–2219.
16. Zhang, H.; Cooper, A.I. Aligned Porous Structures by Directional Freezing. *Adv. Mater.* **2007**, *19*, 1529–1533.
17. Qian, L.; Zhang, H. Controlled freezing and freeze drying: a versatile route for porous and micro-/nano-structured materials. *J. Chem. Technol. Biotechnol.* **2011**, *86*, 172–184.
18. Li, M.; Wu, Z.; Zhang, C.; Lu, S.; Yan, H.; Huang, D.; Ye, H. Study on porous silk fibroin materials. II. Preparation and characteristics of spongy porous silk fibroin materials. *J. Appl. Polym. Sci.* **2001**, *79*, 2192–

2199.

19. Rockwood, D.N.; Preda, R.C.; Yücel, T.; Wang, X.; Lovett, M.L.; Kaplan, D.L. Materials fabrication from Bombyx mori silk fibroin. *Nat. Protoc.* **2011**, *6*, 1612–1631.
20. Greenhalgh, R.D.; Ambler, W.S.; Quinn, S.J.; Medeiros, E.S.; Anderson, M.; Gore, B.; Menner, A.; Bismarck, A.; Li, X.; Tirelli, N.; et al. Hybrid sol–gel inorganic/gelatin porous fibres via solution blow spinning. *J. Mater. Sci.* **2017**, *52*, 9066–9081.
21. Deville, S. The lure of ice-templating: recent trends and opportunities for porous materials. *Scr. Mater.* **2018**, *147*, 119–124.
22. Deville, S. *Freezing colloids: observations, principles, control, and use: applications in materials science, life science, earth science, food science, and engineering*; Springer, 2017;
23. Chatzi, E.G.; Koenig, J.L. Morphology and Structure of Kevlar Fibers: A Review. *Polym. Plast. Technol. Eng.* **1987**, *26*, 229–270.
24. Zhang, F.; Lu, Q.; Yue, X.; Zuo, B.; Qin, M.; Li, F.; Kaplan, D.L.; Zhang, X. Regeneration of high-quality silk fibroin fiber by wet spinning from CaCl2–formic acid solvent. *Acta Biomater.* **2015**, *12*, 139–145.
25. Marsano, E.; Corsini, P.; Arosio, C.; Boschi, A.; Mormino, M.; Freddi, G. Wet spinning of Bombyx mori silk fibroin dissolved in N-methyl morpholine N-oxide and properties of regenerated fibres. *Int. J. Biol. Macromol.* **2005**, *37*, 179–188.
26. Zuo, B.; Liu, L.; Wu, Z. Effect on properties of regenerated silk fibroin fiber coagulated with aqueous methanol/ethanol. *J. Appl. Polym. Sci.* **2007**, *106*, 53–59.
27. Yan, J.; Zhou, G.; Knight, D.P.; Shao, Z.; Chen, X. Wet-Spinning of Regenerated Silk Fiber from Aqueous Silk Fibroin Solution: Discussion of Spinning Parameters. *Biomacromolecules* **2010**, *11*, 1–5.
28. Um, I.C.; Kweon, H.; Lee, K.G.; Ihm, D.W.; Lee, J.-H.; Park, Y.H. Wet spinning of silk polymer: I. Effect of coagulation conditions on the morphological feature of filament. *Int. J. Biol. Macromol.* **2004**, *34*, 89–105.
29. Lee, J.-S.M.; Briggs, M.E.; Hasell, T.; Cooper, A.I. Hyperporous Carbons from Hypercrosslinked Polymers. *Adv. Mater.* **2016**, *28*, 9804–9810.
30. Roberts, A.D.; Kelly, P.; Bain, J.; Morrison, J.J.; Wimpenny, I.; Barrow, M.; Woodward, R.T.; Gresil, M.; Blanford, C.; Hay, S.; et al. Graphene–aramid nanocomposite fibres via superacid co-processing. *Chem. Commun.* **2019**, *55*, 11703–11706.
31. Wei, W.; Zhang, Y.; Zhao, Y.; Shao, H.; Hu, X. Studies on the post-treatment of the dry-spun fibers from regenerated silk fibroin solution: Post-treatment agent and method. *Mater. Des.* **2012**, *36*, 816–822.
32. Guan, G.; Bai, L.; Zuo, B.; Li, M.; Wu, Z.; Li, Y.; Wang, L. Promoted dermis healing from full-thickness skin defect by porous silk fibroin scaffolds (PSFSs). *Biomed. Mater. Eng.* **2010**, *20*, 295–308.
33. Guan, G.; Bai, L.; Zuo, B.; Li, M.; Wu, Z.; Wang, L.; Li, Y. Distinct tissue responses to porous silk fibroin scaffolds (PSFSs) and polyvinyl alcohol (PVA) sponges in vivo. In Proceedings of the 2010 3rd International Conference on Biomedical Engineering and Informatics; IEEE, 2010; Vol. 4, pp. 1668–1672.
34. Guan, G.; Wang, L.; Li, M.; Bai, L. In vivo biodegradation of porous silk fibroin films implanted beneath the skin and muscle of the rat. *Biomed. Mater. Eng.* **2014**, *24*, 789–797.
35. Roberts, A.D.; Zhang, H. Poorly water-soluble drug nanoparticles via solvent evaporation in water-soluble porous polymers. *Int. J. Pharm.* **2013**, *447*, 241–250.
36. Roberts, A.D.; Finnigan, W.; Wolde-Michael, E.; Kelly, P.; Blaker, J.J.; Hay, S.; Breitling, R.; Takano, E.; Scrutton, N.S. Synthetic biology for fibers, adhesives, and active camouflage materials in protection and aerospace. *MRS Commun.* **2019**, 1–19.